Robotica (2011) volume 29, pp. 649–656. © Cambridge University Press 2010
doi:10.1017/S0263574710000524

Simulation of rigid-body impact using the articulated-body algorithm

André Carvalho and Afzal Suleman*

Department of Mechanical Engineering, University of Victoria, 3800 Finnerty Road, Victoria, BC, Canada V8P5C2

(Received in Final Form: August 5, 2010. First published online: September 1, 2010)

SUMMARY

This paper presents a numerical algorithm to model the impact between articulated structures, or between an articulated structure and an object. The proposed algorithm, called impulse articulated-body algorithm (IABA), is based on the ABA but uses impulses and velocities rather than forces and accelerations. The algorithm also inherits the advantages of the ABA: versatility and low computational cost. The IABA provides a method to determine the impact impulse, without increasing the order of the algorithm.

KEYWORDS: Rigid-body dynamics; Impact simulation; Robotics.

1. Introduction

Impact is a severe disturbance to a robot and can cause malfunction or unexpected behavior (especially if the controller is not designed to handle unforeseen changes in the robot state). Because of this, impact analysis has been an area of interest.[1–12]

The simulation of the forward dynamics of articulated structures is a computationally heavy process. One of the fastest algorithms is the articulated-body algorithm (ABA), a versatile $O(n)$ algorithm (where n is the number of links of the articulated structure).[14,15] Originally designed for serial structures (one base link and one end-effector),[13] this algorithm was then adapted to handle tree structures and closed loops.[15–19]

Although versatile, two problems prevent the ABA to handle impact analysis: the state of the robot during impact is a hybrid between the open- and close-loop configurations and the ABA and its derivatives only handle either permanently open- or permanently closed-loop structures, also, these algorithms assume the constrains are always bilateral constrains (the links that close the loop only rotate relatively to each other), while impact constrains are unilateral constrains (only one direction is constrained and the links that close the loop can rotate and move, relatively to each other, in any other direction). The second problem is that impact analysis uses impulses and velocities rather than forces and accelerations.

The proposed impulse ABA (IABA) addresses the problems described above. The IABA algorithm is divided into two parts: the first subalgorithm obtains the variation of the velocities of the links given an impact impulse and the second subalgorithm determines the impact impulse.

The biggest challenge in this work lies on the determination of the impact impulse. The impact impulse equations given by the traditional rigid-body dynamics are well known,[2,3] but these expressions fail when the impacting rigid bodies have their movements constrained (e.g., any articulated structure). One solution to this problem is given by ref. [5], where it is used the fact that the relation between the impact impulse and the variation of the velocity is linear for a given joint configuration. This linear transformation is determined by running an algorithm similar to the velocity/impulse version of the ABA presented in this paper, for a known arbitrary "test" impact impulse, which results in a matrix that premultiplies the variation of the velocity (the difference between the velocity before and after the impact). After the transformation matrix is determined it must be inverted in order to get the impact impulse. According to this method, an algorithm with a computational cost similar to the ABA must be run four times at each sample time to complete the calculations: one for each of the three components of the "test" impact impulse, and a fourth to get the results. In addition to the high number of computations, the method does not guarantee that the linear transformation matrix obtained is nonsingular, especially when one of the intervening bodies is fixed (e.g., a ground plane).

The focus of this paper is to find a less computationally expensive, analytical model for the impact impulse using the properties and advantages of the ABA.

The outline of this paper is as follows. First, we describe the mathematical model behind the ABA. Then, we develop the impulse version of the ABA. We also present the method to determine the impact impulse between two articulated structures or between an articulated structure and a fixed object. In the immediately following section, the extension of the IABA for tree structures is presented. Finally, we introduce some results, as well as an estimate of the computational cost.

2. Articulated-Body Algorithm

2.1. Basic equations

The ABA is currently the fastest serial processing algorithm for a series of rigid-bodies interconnected by joints. It is compared against other leading algorithms – the

* Corresponding author. E-mail: suleman@uvic.ca

https://doi.org/10.1017/S0263574710000524 Published online by Cambridge University Press

Table I. Fastest algorithms as function of number of bodies (NB) and number of processors (NP)[14].

	$N_B = 10$	$N_B = 100$	$N_B = 1000$
$N_P = 1$	ABA	ABA	ABA
$N_P = 10$	HDIA	HDIA	HDIA
$N_P = 100$	–	HDIA/DCA	HDIA/DCA
$N_P = 1000$	–	–	DCA

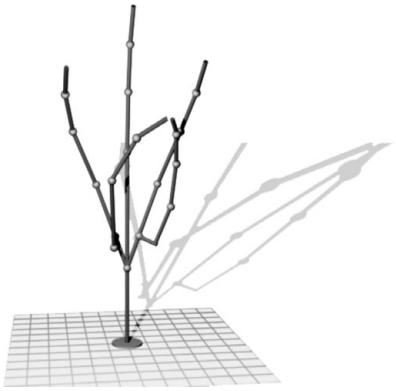


Fig. 1. Joint–link model of a human hand.

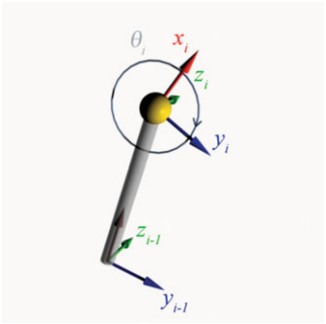


Fig. 2. Link with joint and reference frames.

divide-and-conquer algorithm (DCA),[15] and the hybrid direct/iterative algorithm (HDIA)[19] – in Table I.

Developed by Featherstone,[13] this algorithm solves a linear system of n equations, while remaining $O(n)$, using the Newton–Euler vector dynamics relations.

The cornerstone of the ABA is the treatment of a structure link by link, rather than as a whole. Selecting a link from the structure depicted in Fig. 1 and defining the reference frames, as shown in Fig. 2:

the equations for the velocities and acceleration of the i-frame are given by (1) to (5).

$$\mathbf{v}_i^O = \mathbf{R}_{i-1}^i \mathbf{v}_{i-1}^O + \boldsymbol{\omega}_{i-1} \times \mathbf{r}_{i-1}^L, \tag{1}$$

$$\boldsymbol{\omega}_i = \mathbf{R}_{i-1}^i \boldsymbol{\omega}_{i-1} + \boldsymbol{\phi}_i \dot{\theta}_i, \tag{2}$$

$$\mathbf{a}_i^O = \mathbf{R}_{i-1}^i \big(\mathbf{a}_{i-1}^O + \boldsymbol{\alpha}_{i-1} \times \mathbf{r}_{i-1}^L + \boldsymbol{\omega}_{i-1} \times \big(\boldsymbol{\omega}_{i-1} \times \mathbf{r}_{i-1}^L\big)\big), \tag{3}$$

$$\boldsymbol{\alpha}_i = \mathbf{R}_{i-1}^i \boldsymbol{\alpha}_{i-1} + \boldsymbol{\phi}_i \ddot{\theta}_i + \boldsymbol{\omega}_i \times (\boldsymbol{\phi}_i \dot{\theta}_i), \tag{4}$$

$$\mathbf{a}_i^{CM} = \mathbf{a}_i^O + \boldsymbol{\alpha}_i \times \mathbf{r}_i^{CM} + \boldsymbol{\omega}_i \times \big(\boldsymbol{\omega}_i \times \mathbf{r}_i^{CM}\big), \tag{5}$$

where $\mathbf{R}_{i-1}^i$ is the rotation matrix from the (i-1)-frame to the i-frame, $\mathbf{v}_i^O$ is the translation velocity at the origin of the i-frame, $\boldsymbol{\omega}_i$ is the angular velocity of the i-frame, $\mathbf{r}_{i-1}^L$ is the position of the origin of the i-frame relatively to the origin of the (i-1)-frame, $\dot{\theta}_i$ is the norm of the angular velocity of the joint to which the i-frame is attached to, $\boldsymbol{\phi}_i$ is an unit vector, representing the direction of the rotation axis of the joint, $\mathbf{a}_i^O$ is the translation acceleration at the origin of the i-frame, $\boldsymbol{\alpha}_i$ is the angular acceleration of the i-frame, $\ddot{\theta}_i$ is the norm of the angular acceleration of the joint at the i-frame, $\mathbf{a}_i^{CM}$ is the linear acceleration at the center of mass (CM) of the link, and $\mathbf{r}_{i-1}^{CM}$ is the position of the CM relatively to the (i-1)-frame. Note that all the quantities in bold represent vector or matrix quantities.

Based on Fig. 2, we can also define the force and moment balances (6) and (7):

$$\sum \mathbf{F} = \mathbf{F}_{i-1} + \mathbf{F}_i = m_{i-1} \mathbf{a}_{i-1}^{CM}, \tag{6}$$

$$\sum \mathbf{M} = \mathbf{M}_{i-1} + \mathbf{M}_i + \mathbf{r}_{i-1}^L \times \mathbf{F}_i = \dot{\mathbf{H}}_{i-1}^O, \tag{7}$$

where $\mathbf{F}_i$ and $\mathbf{M}_i$ are external forces and moments, respectively, m_{i-1} is the mass of the link, and $\dot{\mathbf{H}}_{i-1}^O$ is the time derivative of the angular momentum at the origin of the (i-1)-frame, given by (8).

$$\dot{\mathbf{H}}_{i-1}^O = \mathbf{I}_{i-1}^O \boldsymbol{\alpha}_{i-1} + \mathbf{r}_{i-1}^{CM} \times m_{i-1} \mathbf{a}_{i-1}^O + \boldsymbol{\omega}_{i-1} \times \mathbf{I}_{i-1}^O \boldsymbol{\omega}_{i-1}, \tag{8}$$

where $\mathbf{I}_{i-1}^O$ is the inertia tensor of the link calculated at the origin of the (i-1)-frame.

2.2. *Spatial quantities and articulated-body inertia*

The ABA introduces a new notation – the spatial vectors. Spatial vectors assemble on a single vector both linear and angular parts of a quantity (9):

$$\hat{\mathbf{v}}_i = \begin{bmatrix} \mathbf{v}_i^O \\ \omega_i \end{bmatrix}, \quad \hat{\mathbf{a}}_i = \begin{bmatrix} \mathbf{a}_i^O \\ \boldsymbol{\alpha}_i \end{bmatrix}, \quad \hat{\mathbf{F}}_i = \begin{bmatrix} \mathbf{F}_i \\ \mathbf{M}_i \end{bmatrix}, \tag{9}$$

where $\hat{\mathbf{v}}_i$, $\hat{\mathbf{a}}_i$, $\hat{\mathbf{F}}_i$ are the spatial velocity, spatial acceleration, and spatial force at the i-frame, respectively. Note that original definition of spatial vectors given by Featherstone[12] was reversed in this paper for convenience.[4]

With this new notation, Eqs. (1) to (8) become Eqs. (10) to (12).

$$\hat{\mathbf{v}}_i = \hat{\mathbf{X}}_{i-1}^i \hat{\mathbf{v}}_{i-1} + \hat{\boldsymbol{\phi}}_i \dot{\theta}_i, \tag{10}$$

$$\hat{\mathbf{a}}_i = \hat{\mathbf{X}}_{i-1}^i \hat{\mathbf{a}}_{i-1} + \hat{\boldsymbol{\phi}}_i \ddot{\theta}_i + \hat{\mathbf{C}}_i, \tag{11}$$

$$\hat{\mathbf{F}}_i - \big(\hat{\mathbf{X}}_i^{i+1}\big)^T \hat{\mathbf{F}}_{i+1} = \hat{\mathbf{I}}_i \hat{\mathbf{a}}_i + \hat{\boldsymbol{\beta}}_i, \tag{12}$$

where $\hat{\mathbf{X}}_{i-1}^i$ is the spatial transformation matrix that converts spatial quantities from the (i-1)-frame to the i-frame (13), $\hat{\boldsymbol{\phi}}_i$ is a unit vector six-dimensional vector, defining the axis of the joint at the i-frame, $\hat{\mathbf{C}}_i$ is the centripetal component of the spatial acceleration (14), $\hat{\mathbf{I}}_i$ is the spatial inertia matrix (15),

https://doi.org/10.1017/S0263574710000524 Published online by Cambridge University Press

and $\hat{\boldsymbol{\beta}}_i$ is the spatial force bias (16):

$$\hat{\mathbf{X}}_{i-1}^{i} = \begin{bmatrix} \mathbf{R}_{i-1}^{i} & -\mathbf{R}_{i-1}^{i}\mathbf{S}_{i-1}^{\mathbf{r}_{i-1}^{L}} \\ \mathbf{0} & \mathbf{R}_{i-1}^{i} \end{bmatrix}, \tag{13}$$

$$\hat{\mathbf{C}}_i = \begin{bmatrix} R_{i-1}^{i}\left(\boldsymbol{\omega}_{i-1} \times \left(\boldsymbol{\omega}_{i-1} \times r_{i-1}^{L}\right)\right) \\ \boldsymbol{\omega}_i \times \boldsymbol{\phi}_i \dot{\theta}_i \end{bmatrix}, \tag{14}$$

$$\hat{\mathbf{I}}_i = \begin{bmatrix} m_i \mathbf{1} & -m_i \mathbf{S}_i^{\mathbf{r}_i^{CM}} \\ m_i \mathbf{S}_i^{\mathbf{r}_i^{CM}} & \mathbf{I}_i^{O} \end{bmatrix}, \tag{15}$$

$$\hat{\boldsymbol{\beta}}_i = \begin{bmatrix} m_i \boldsymbol{\omega}_i \times \left(\boldsymbol{\omega}_i \times \mathbf{r}_i^{CM}\right) \\ \boldsymbol{\omega}_i \times \mathbf{I}_i^{O} \boldsymbol{\omega}_i \end{bmatrix}, \tag{16}$$

where $\mathbf{S}_i^{\mathbf{r}_{i-1}^{L}}$ and $\mathbf{S}_i^{\mathbf{r}_{i-1}^{CM}}$ are the skew-symmetric matrices that represent the cross products $\mathbf{r}_{i-1}^{L}\times$ and $\mathbf{r}_{i-1}^{CM}\times$, respectively.

The spatial force bias, $\hat{\boldsymbol{\beta}}_i$, comes from the fact that the balance of forces, (12), is no longer done at the CM, being done, instead, at the origin of the base frame.

The ABA also introduces the articulated-body inertia, $\hat{\mathbf{I}}_i^A$, and force bias, $\hat{\boldsymbol{\beta}}_i^A$, defined by (17) and (18):[13,14]

$$\hat{\mathbf{I}}_{i-1}^{A} = \hat{\mathbf{I}}_{i-1} + \left(\hat{\mathbf{X}}_{i-1}^{i}\right)^{T} \mathbf{N}_i \hat{\mathbf{X}}_{i-1}^{i}, \tag{17}$$

$$\hat{\boldsymbol{\beta}}_{i-1}^{A} = \hat{\boldsymbol{\beta}}_{i-1} + \left(\hat{\mathbf{X}}_{i-1}^{1}\right)^{T} \left(\hat{\boldsymbol{\beta}}_i^{A} + \mathbf{N}_i \hat{\mathbf{C}}_i + \mathbf{n}_i \mathbf{M}_i^{-1} \tau_i^{*}\right), \tag{18}$$

where τ_i^* is the applied torque to the joint adjusted for the dynamic forces (damping and elasticity of the joint), and $\mathbf{N}_i$, $\mathbf{n}_i$, and $\mathbf{M}_i$ are auxiliary variable defined by

$$\mathbf{N}_i = \hat{\mathbf{I}}_i^{A} - \mathbf{n}_i \mathbf{M}_i^{-1} \mathbf{n}_i^{T}, \tag{19}$$

$$\mathbf{n}_i = \hat{\mathbf{I}}_i^{A} \hat{\boldsymbol{\phi}}_i, \tag{20}$$

$$\mathbf{M}_i = \hat{\boldsymbol{\phi}}_i^{T} \hat{\mathbf{I}}_i^{A} \hat{\boldsymbol{\phi}}_i. \tag{21}$$

Because the articulated-body inertia and force bias account for the dynamic behavior of the link in study and the effect of the movement of the upper links (all the links connected to the link top frame), the balance of forces defined by (12) is no longer explicitly dependent on the upper links quantities (22):

$$\hat{\mathbf{F}}_i = \hat{\mathbf{I}}_i^{A} \hat{\mathbf{a}}_i + \hat{\boldsymbol{\beta}}_i^{A}. \tag{22}$$

With Eq. (22) the system of equations formed by the equation of the dynamics changes from full rank to a triangular system. Hence, obtaining a solution requires $O(n)$ operations rather than $O(n^2)$.[13] The last quantity to be determined and the goal of the ABA is the joint angular acceleration and is given by

$$\ddot{\theta}_i = \left(\hat{\boldsymbol{\phi}}_i^{T} \hat{\mathbf{I}}_i^{A} \hat{\boldsymbol{\phi}}_i\right)^{-1} \left(\left(\tau_i^{*} - \hat{\boldsymbol{\phi}}_i^{T} \hat{\boldsymbol{\beta}}_i^{A}\right) - \hat{\boldsymbol{\phi}}_i^{T} \hat{\mathbf{I}}_i^{A} \left(\hat{\mathbf{X}}_{i-1}^{i} \hat{\mathbf{a}}_{i-1} + \hat{\mathbf{C}}_i\right)\right). \tag{23}$$

3. Impulse Articulated-Body Algorithm

3.1. Velocity/impulse ABA

According to the theory of rigid-body dynamics, the impact is instantaneous. Since the duration of the impact is zero, there is a discontinuity in the velocities and accelerations of the rigid bodies. Therefore, an infinite force must be exerted at the point of contact to create a finite impulse (20).

$$\Delta \mathbf{i} = \mathbf{F} \Delta t, \tag{24}$$

where $\mathbf{i}$ is the impulse. Because of this infinite force, the simulation of the impact needs to be done on an impulse-based ABA rather than on the traditional force-based ABA.

The IABA has its foundation on the time integral of (12), given by

$$\hat{\mathbf{i}}_{i-1} - \left(\hat{\mathbf{X}}_{i-1}^{i}\right)^{T} \hat{\mathbf{i}}_i = \hat{\mathbf{I}}_{i-1} \Delta \hat{\mathbf{v}}_{i-1}, \tag{25}$$

where $\hat{\mathbf{i}}_i$ is the spatial impulse (defined similarly to (9), using the linear impulse and angular impulse), and $\Delta \hat{\mathbf{v}}_i$ is the time variation of the spatial velocity.

The development of the IABA is performed in the same way as Featherstone's ABA.[13] Starting from the last link in the chain we have (26)

$$\hat{\mathbf{i}}_i = \hat{\mathbf{I}}_i \Delta \hat{\mathbf{v}}_i + \hat{\boldsymbol{\gamma}}_i, \tag{26}$$

where $\hat{\boldsymbol{\gamma}}_i$ is the spatial impulse bias, which comprises all external impulses applied to the link. Since (26) represents the last link in the chain, the spatial inertia and impulse bias are equal to the articulated-body inertia and articulated-body impulse bias (defined ahead), yielding

$$\hat{\mathbf{i}}_i = \hat{\mathbf{I}}_i^{A} \Delta \hat{\mathbf{v}}_i + \hat{\boldsymbol{\gamma}}_i^{A}, \tag{27}$$

where the quantities superscripted with an "A" represent the articulated-body quantities.

Replacing the variation of the spatial velocity of the link with (28), we obtain (29)

$$\Delta \hat{\mathbf{v}}_i = \hat{\mathbf{X}}_{i-1}^{i} \Delta \hat{\mathbf{v}}_{i-1} + \hat{\boldsymbol{\phi}}_i \Delta \dot{\theta}_i. \tag{28}$$

Note that (28) is the time-varying version of (10).

$$\hat{\mathbf{i}}_i = \hat{\mathbf{I}}_i^{A} \left(\hat{\mathbf{X}}_{i-1}^{i} \Delta \hat{\mathbf{v}}_{i-1} + \hat{\boldsymbol{\phi}}_i \Delta \dot{\theta}_i\right) + \hat{\boldsymbol{\gamma}}_i^{A}. \tag{29}$$

Premultiplying (29) by $\hat{\boldsymbol{\phi}}_i^{T}$ and solving for the variation of the joint angular velocity results in (30).

$$\Delta \dot{\theta}_i = \left(\hat{\boldsymbol{\phi}}_i^{T} \hat{\mathbf{I}}_i^{A} \hat{\boldsymbol{\phi}}_i\right)^{-1} \left(\iota_i - \hat{\boldsymbol{\phi}}_i^{T} \hat{\boldsymbol{\gamma}}_i^{A} - \hat{\boldsymbol{\phi}}_i^{T} \hat{\mathbf{I}}_i^{A} \hat{\mathbf{X}}_{i-1}^{i} \Delta \hat{\mathbf{v}}_{i-1}\right), \tag{30}$$

where ι_i is the angular impulse applied to the joint, which is the impulse due to the applied torque. ι_i results from $\hat{\boldsymbol{\phi}}_i^{T} \hat{\mathbf{i}}_i$ in the same way that τ_i^* results from $\hat{\boldsymbol{\phi}}_i^{T} \mathbf{F}_i$.

Replacing (30) back into (29), we obtain

$$\hat{\mathbf{i}}_i = \mathbf{N}_i \hat{\mathbf{X}}_{i-1}^{i} \Delta \hat{\mathbf{v}}_{i-1} - \mathbf{n}_i \mathbf{M}_i^{-1} \hat{\boldsymbol{\phi}}_i^{T} \hat{\boldsymbol{\gamma}}_i^{A} + \hat{\boldsymbol{\gamma}}_i^{A}, \tag{31}$$

where $\mathbf{N}_i$, $\mathbf{n}_i$, and $\mathbf{M}_i$ are also defined by (19), (20), and (21), respectively.

https://doi.org/10.1017/S0263574710000524 Published online by Cambridge University Press

Substituting (31) in (25) and applying the same simplifications used in the demonstration of the ABA,[13] we obtain the equation for the articulated-body impulse bias, (32), and the equation for the articulated-body inertia, which is equal to (17).

$$\hat{\gamma}_{i-1}^{A} = \left(\hat{\mathbf{X}}_{i-1}^{i}\right)^{T}\left(\mathbf{n}_i\mathbf{M}_i^{-1}\iota_i + \left(1 - \mathbf{n}_i\mathbf{M}_i^{-1}\hat{\boldsymbol{\phi}}_i^{T}\right)\hat{\gamma}_i^{A}\right). \quad (32)$$

Since the theoretical impact is instantaneous, the external impulse ι_i is zero, simplifying (32) into (33).

$$\hat{\gamma}_{i-1}^{A} = \left(\hat{\mathbf{X}}_{i-1}^{i}\right)^{T}\left(1 - \mathbf{n}_i\mathbf{M}_i^{-1}\hat{\boldsymbol{\phi}}_i^{T}\right)\hat{\gamma}_i^{A}. \quad (33)$$

3.2. *Impact impulse for constrained rigid bodies*

The impulse generated by the impact of two rigid bodies depends exclusively on the normal component of the relative velocity of the bodies (for frictionless impact only), their masses and inertias. The analytical expression for the impact impulse of two rigid bodies (denoted here "1" and "2") is given by (34):[3]

$$\|\mathbf{i}_c\| = -(1+e)\frac{\left(\mathbf{v}_2^{-} - \mathbf{v}_1^{-}\right)\cdot\mathbf{n}}{\sum_{k=1}^{2}\left(\frac{1}{m_k} + \mathbf{n}\cdot\left(\bar{\mathbf{I}}_k^{-1}\left(\mathbf{r}_k\times\mathbf{n}\right)\times\mathbf{r}_k\right)\right)}, \quad (34)$$

where $\mathbf{i}_c$ is the impact impulse, e is the coefficient of restitution, $\mathbf{v}_1^{-}$ and $\mathbf{v}_2^{-}$ are the linear velocities immediately before the impact, $\mathbf{n}$ is the unitary normal to the contact plane, $\mathbf{r}_k$ is the position of the impact point relatively to CM of the k body, and m_k and $\bar{\mathbf{I}}_k$ are the mass and the inertia tensor at the CM of the body k.

Equation (34), although generic, fails when used to simulate impacts with articulated structures. This equation can only be applied if the two intervening objects are rigid as a whole and not by parts (like articulated structures), because it only uses the total inertia of the objects disregarding any inner dynamics. Also, this equation does not support constrained objects, because one of its basic assumptions is that the rigid objects are free to move in their environment.[2–5]

In order to solve this problem, we must determine the extension of (34) for articulated rigid-bodies structures. The first step is the elimination of the recursive form of (33), knowing that the first nonzero $\hat{\gamma}^A$ in the recursion is the one corresponding to the impacting link (35).[4]

$$\hat{\gamma}_{n_c}^{A} = -\left(\hat{\mathbf{X}}_{n_c}^{C}\right)^{T}\hat{\mathbf{i}}_c, \quad (35)$$

where n_c is the index of the colliding link, $\hat{\mathbf{X}}_{n_c}^{C}$ is the spatial transformation matrix from the origin of the base frame of the colliding link to the collision point, and $\hat{\mathbf{i}}_c$ is the spatial collision impulse.

The nonrecursive form of (33) is given by the following equation:

$$\hat{\gamma}_i^{A} = \left(\prod_{j=i+1}^{n_c}\mathbf{A}_j\right)\hat{\gamma}_{n_c}^{A}, \quad (36)$$

where $\mathbf{A}_j$ is an auxiliary variable defined by

$$\mathbf{A}_i = \left(\hat{\mathbf{X}}_{i-1}^{i}\right)^{T}\left(1 - \mathbf{n}_i\mathbf{M}_i^{-1}\hat{\boldsymbol{\phi}}_i^{T}\right). \quad (37)$$

Merging (28) with (36) and rearranging the final equation to explicit the articulated-body impulse bias, we obtain

$$\Delta\hat{\mathbf{v}}_i = \mathbf{A}_i^{T}\Delta\hat{\mathbf{v}}_{i-1} - \boldsymbol{\psi}_i\hat{\gamma}_i^{A} \quad (38)$$

where

$$\boldsymbol{\psi}_i = \hat{\boldsymbol{\phi}}_i\mathbf{M}_i^{-1}\hat{\boldsymbol{\phi}}_i^{T}. \quad (39)$$

Removing the recursion from (38), we obtain the relation between the variation of the velocity on the impacting link and the articulated-body impulse bias (36).

$$\Delta\hat{\mathbf{v}}_{n_c} = -\sum_{i=1}^{n_c}\left(\left(\prod_{j=i+1}^{n_c}\mathbf{A}_j\right)^{T}\boldsymbol{\psi}_i\left(\prod_{j=i+1}^{n_c}\mathbf{A}_j\right)\right). \quad (40)$$

Analyzing the computational cost of (36), one reaches the conclusion that it is a $O(n^2)$ equation, which is highly detrimental to the performance of the algorithm. The solution is to transform (40) back into a recursive equation (41).

$$\Delta\hat{\mathbf{v}}_{n_c} = -\boldsymbol{\Psi}_{n_c}\hat{\gamma}_{n_c}^{A}, \quad (41)$$

where

$$\boldsymbol{\Psi}_i = \mathbf{A}_i^{T}\boldsymbol{\Psi}_{i-1}\mathbf{A}_i + \boldsymbol{\psi}_i, \quad (42)$$

The starting point for (42) is $\boldsymbol{\Psi}_1 = \boldsymbol{\psi}_1$. The main advantage of (42) is that it recovers the $O(n)$ performance.

Replacing (35) into (41) and premultiplying it by $\hat{\mathbf{X}}_{n_c}^{C}$ to get the variation of the velocity at the contact point, we obtain

$$\hat{\mathbf{X}}_{n_c}^{C}\Delta\hat{\mathbf{v}}_{n_c} = \hat{\mathbf{X}}_{n_c}^{C}\boldsymbol{\Psi}_{n_c}\left(\hat{\mathbf{X}}_{n_c}^{C}\right)^{T}\hat{\mathbf{i}}_c. \quad (43)$$

Since we are assuming frictionless impact, only the normal component of the variation of the velocity is affected by the impulse, which has the same direction as the normal. Premultiplying (43) by the transpose of the normal direction (converted to a spatial vector) and solving for the impact impulse norm, we have

$$\|\hat{\mathbf{i}}_c\| = \frac{\hat{\mathbf{n}}_{n_c}^{T}\hat{\mathbf{X}}_{n_c}^{C}\Delta\hat{\mathbf{v}}_{n_c}}{\hat{\mathbf{n}}_{n_c}^{T}\hat{\mathbf{X}}_{n_c}^{C}\boldsymbol{\Psi}_{n_c}\left(\hat{\mathbf{X}}_{n_c}^{C}\right)^{T}\hat{\mathbf{n}}_{n_c}}, \quad (44)$$

where $\hat{\mathbf{n}}_{n_c}$ is the spatial version of the normal of the contact plane at the impacting link.

The velocity (of the impact point) immediately after the impact is directly proportional to the velocity immediately before the impact[3] and is given by

$$\hat{\mathbf{n}}_{n_c}^{T}\hat{\mathbf{X}}_{n_c}^{C}\hat{\mathbf{v}}_{n_c}^{+} = -e\hat{\mathbf{n}}_{n_c}^{T}\hat{\mathbf{X}}_{n_c}^{C}\hat{\mathbf{v}}_{n_c}^{-}, \quad (45)$$

where $\hat{\mathbf{v}}_{n_c}^{+}$ and $\hat{\mathbf{v}}_{n_c}^{-}$ are the spatial velocities of the impacting link immediately after and before the impact, respectively.

https://doi.org/10.1017/S0263574710000524 Published online by Cambridge University Press

Using (45), we can express the norm of the impact impulse exclusively with known quantities (46).

$$\|\hat{\mathbf{i}}_c\| = -(1+e)\frac{\hat{\mathbf{n}}_{n_c}^T \hat{\mathbf{X}}_{n_c}^C \hat{\mathbf{v}}_{n_c}^-}{\hat{\mathbf{n}}_{n_c}^T \hat{\mathbf{X}}_{n_c}^C \boldsymbol{\Psi}_{n_c} \left(\hat{\mathbf{X}}_{n_c}^C\right)^T \hat{\mathbf{n}}_{n_c}}, \tag{46}$$

Equation (42) gives us the impact norm for the collision of an articulated structure with the ground or an object with a mass several orders of magnitude higher. However, it can be modified for a more generic situation such as the impact between two articulated structures (47).

$$\|\hat{\mathbf{i}}_c\| = -(1+e)\frac{{}^2\hat{\mathbf{n}}_{n_c}^T\, {}^2\hat{\mathbf{X}}_{n_c}^C\, {}^2\hat{\mathbf{v}}_{n_c}^- - {}^1\hat{\mathbf{n}}_{n_c}^T\, {}^1\hat{\mathbf{X}}_{n_c}^C\, {}^1\hat{\mathbf{v}}_{n_c}^-}{\sum_{i=1}^{2}\left({}^i\hat{\mathbf{n}}_{n_c}^T\, {}^i\hat{\mathbf{X}}_{n_c}^C\, {}^i\boldsymbol{\Psi}_{n_c}\left({}^i\hat{\mathbf{X}}_{n_c}^C\right)^T {}^i\hat{\mathbf{n}}_{n_c}\right)}, \tag{47}$$

where the two articulated structures are differentiated by the "1" and "2" left superscripts.

3.3. Algorithm

The determination of the impact impulse introduces some changes into the IABA algorithm described above.

(1) *Articulated-body inertia cycle:* Starting at the last link of the chain, compute the articulated-body inertias for the impact joint configuration.
(2) *Impact impulse:* Starting at the first link, calculate the $\boldsymbol{\Psi}$ matrices for each link up to the impacting link. Compute the impact impulse from these matrices.
(3) *Articulated–body impulse bias cycle:* Starting at the impacting link, compute the articulated-body impulse bias.
(4) *Velocities cycle:* Starting at the first link, compute the velocities of each link using (28) and (30). If the first link is attached to the surroundings, the variation of the velocity of the base link is zero.

4. IABA for Tree Structures

Tree structures are articulated structures that have joints with several links instead of just two. This added complexity brings some changes to the ABA[4,15,16,18] and to the IABA.

The demonstration process follows the same steps as for the IABA. However, one must consider more than one child link (links connection above the joint).

$$\hat{\mathbf{i}}_{i-1} - \sum_{j=1}^{N_j}\left({}^j\hat{\mathbf{X}}_{i-1}^i\right)^T {}^j\hat{\mathbf{i}}_i = \hat{\mathbf{I}}_{i-1}\Delta\hat{\mathbf{v}}_{i-1}, \tag{48}$$

where j and N_j are the index and the number of child links of the current joint. Following the demonstration of the IABA, one obtains the new definitions for the articulated-body inertia and impulse bias:

$$\hat{\mathbf{I}}_{i-1}^A = \sum_{j=1}^{N_j}\left({}^j\hat{\mathbf{I}}_{i-1} + \left({}^j\hat{\mathbf{X}}_{i-1}^i\right)^T {}^j\mathbf{N}_i\, {}^j\hat{\mathbf{X}}_{i-1}^i\right) \tag{49}$$

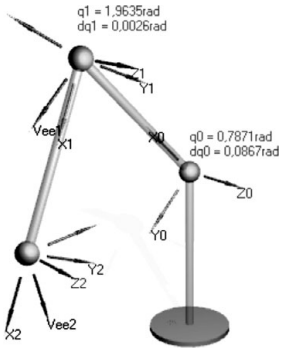


Fig. 3. Initial position of the serial structure used in the first example.

$$\hat{\boldsymbol{\gamma}}_{i-1}^A = \sum_{j=1}^{N_j}\left(\left(\hat{\mathbf{X}}_{i-1}^i\right)^T\left(1 - {}^j\mathbf{n}_i\, {}^j\mathbf{M}_i^{-1}\, {}^j\hat{\boldsymbol{\phi}}_i^T\right){}^j\hat{\boldsymbol{\gamma}}_i^A\right). \tag{50}$$

All the other equations remain unaltered.

The impact impulse is determined using the same equations of the IABA, but Eq. (42) now has to follow the path from the base of the structure to the impacting link, instead of going through all links.

5. Results

In this section, we shall present the results obtained from two test cases along with a study on the computational cost of the algorithm.

5.1. Simulation tests

The simplest test that can be done to the algorithm is the impact with ground plane of a falling serial structure while subjected to its own weight. The first test is done with a two-link structure with one degree of freedom (DoF) per joint, like the one shown in Fig. 3.

All links have the same length and consequently only the tip of the end-effector can touch the ground. The coefficient of restitution is 1, denoting a fully elastic collision. The starting position of the structure and the subsequent path of the joints on the *XZ*-plane are shown in Fig. 4, the linear velocities of the frames 1 and 2 (Fig. 3) are shown in Figs. 5 and 6, respectively, and the evolution of the joint positions can be seen in Fig. 7.

It can be seen in Figs. 4–6 that there are four impacts with the ground plane. Because the collisions are fully elastic, the normal component of the velocity of the impact point (*Z* component of Fig. 6) maintains its value through the impact, but with a reversed signal, creating a discontinuity. There are also discontinuities on the tangential component (*X* component of Fig. 6) that result from the couplings present in the structure and not the impact itself.

The second test is similar to the first one but with a more complex structure with five links. The starting position of the structure and the movement paths can be seen in Fig. 8, the linear velocities of the impacting links are shown in Figs. 9–11 (Note: the numbering scheme of the reference frames is similar to the one depicted in Fig. 3). Finally the path of the structure in joint space is shown in Fig. 12.

https://doi.org/10.1017/S0263574710000524 Published online by Cambridge University Press

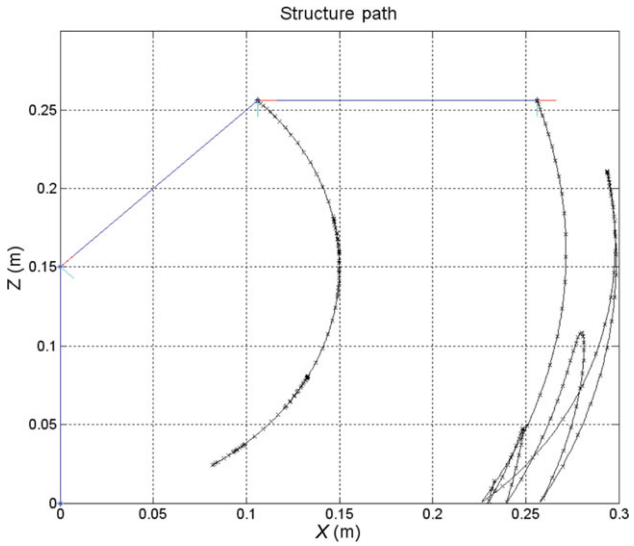


Fig. 4. Initial position and path of the structure.

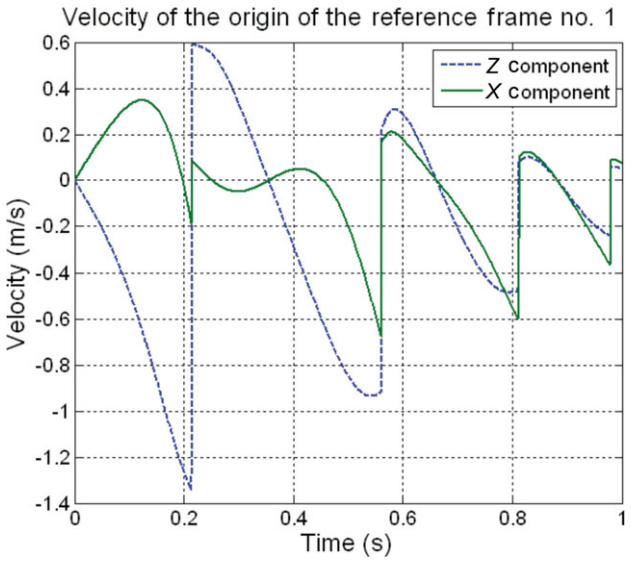


Fig. 5. Linear velocity at the tip of the first mobile link.

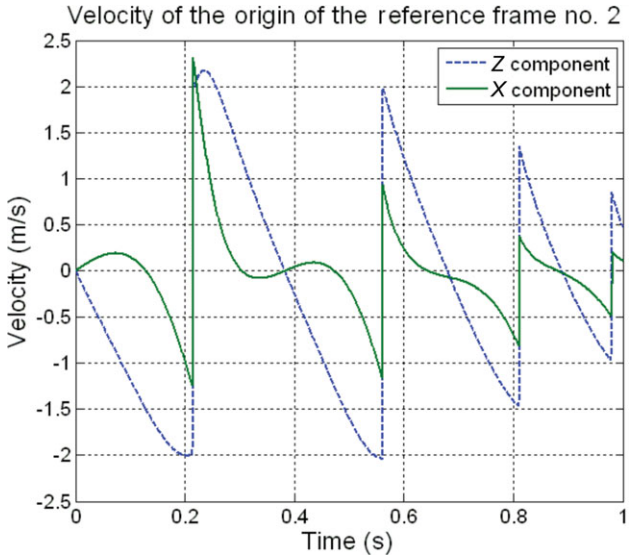


Fig. 6. Linear velocity at the tip of the second mobile link.

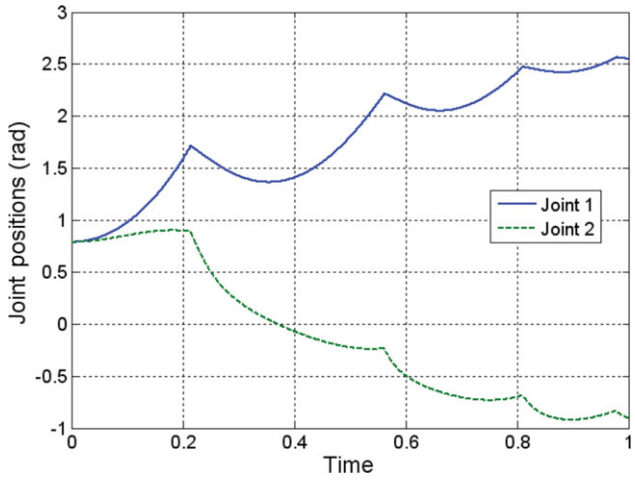


Fig. 7. Path of the structure in joint space.

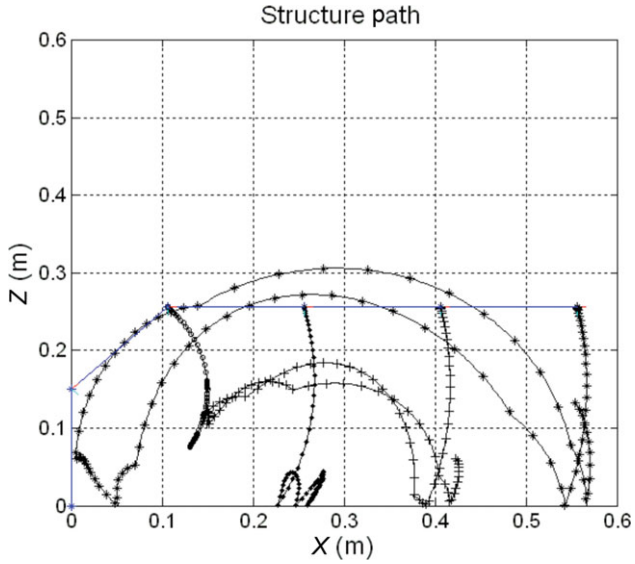


Fig. 8. Initial position and path of the five-link structure test.

The main difference between the results from these tests is that on the first one only one link has the possibility of hitting the ground plane while on the second one there are three links that can do so. The only way to know which link collides and the sequence of collisions (from the plots shown in Figs. 9–11) is to see where the discontinuities are symmetric around the origin (this characteristic is only present in fully elastic collisions). The sequence of collisions is the following: link 4, 3, 2, 2, 4, 2, 2, 2, and 4.

5.2. *Computational cost*

The computational cost of an algorithm depends heavily on how it was implemented and on the optimizations done (symmetry of the matrices, redundant operations, sequence of operations). If we perform an operation count on the algorithm – the basic operations being summations, subtractions, scalar products, and divisions – we can determine its level of complexity (Table II).

https://doi.org/10.1017/S0263574710000524 Published online by Cambridge University Press

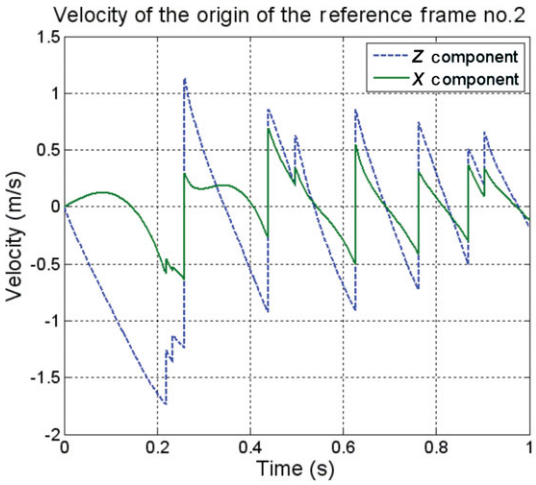


Fig. 9. Linear velocity at the tip of the second mobile link.

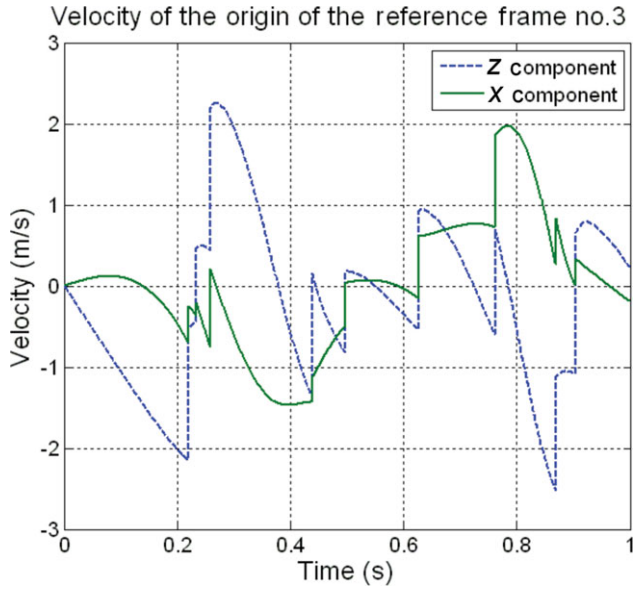


Fig. 10. Linear velocity at the tip of the third mobile link.

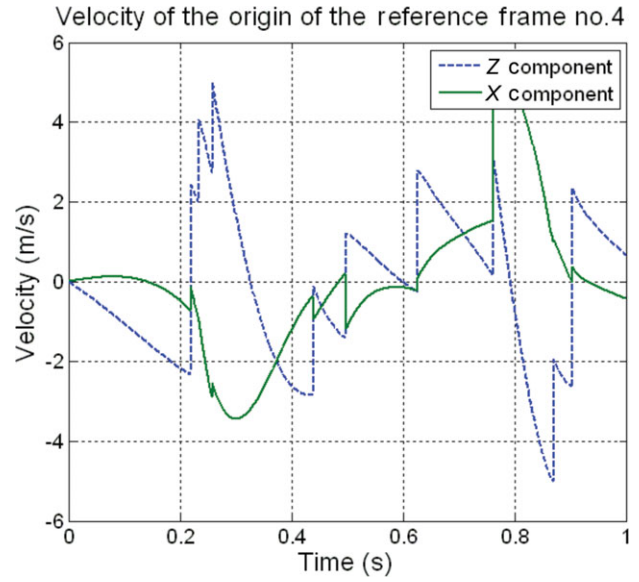


Fig. 11. Linear velocity at the tip of the fourth mobile link.

Table II. Computational cost of the proposed algorithm as function of the number of links (n).

	Number of operations
IABA (articulated-body inertias)	$984n$
Impact impulse	$207 + 870n$
IABA (impulse bias and velocities)	$649n$
Total	$2503n + 207$

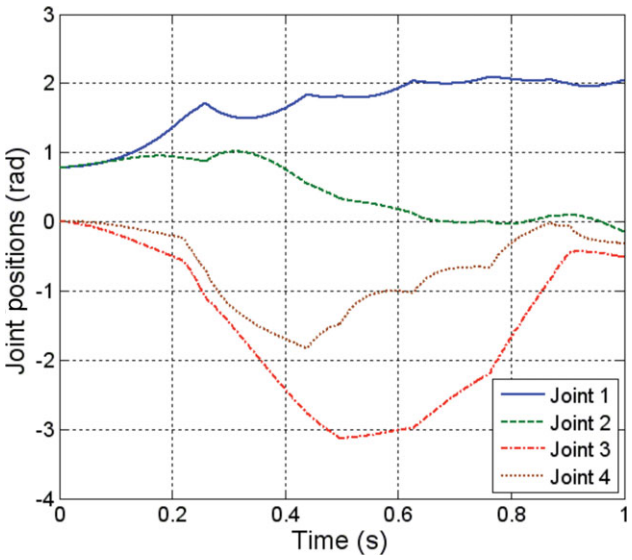


Fig. 12. Path of the structure in joint space.

6. Conclusions

In this paper, we proposed a new algorithm, based on the ABA, to calculate the effect of impacts between a serial/tree articulated structure and its environment, while retaining the $O(n)$ complexity. The IABA is divided into two main parts: the counterpart of the ABA for velocities and impulses, and the determination of the impact impulse. The advantages of using the IABA and the proposed impact impulse equations are twofold.

- The inherited versatility. Like the IABA and ABA, the impact impulse equation can handle both serial and tree structures.
- It can be integrated almost seamlessly into the ABA so that no additional runs of the algorithm are required.

Future work will focus on investigating the effect of the precision of impact detection on the results.

Acknowledgments

This work was supported in part by the *Fundação para a Ciência e Tecnologia* (FCT) under Grant SFRH/BD/22861/2005.

References

1. D. Baraff, "Fast Contact Force Computation for Nonpenetrating Rigid Bodies," *Computer Graphics Proceedings, Annual Conference Series* (Orlando, 1994) pp. 23–34.
2. D. Baraff, "An Introduction to Physically Base Modeling: Rigid Body Simulation I – Unconstrained Rigid Body Dynamics," *Siggraph'97 Course Notes* (1997), pp. D1-D31.

https://doi.org/10.1017/S0263574710000524 Published online by Cambridge University Press

3. D. Baraff, "An Introduction to Physically Base Modeling: Rigid Body Simulation II – Nonpenetration Constrains," *Siggraph'97 Course Notes* (1997), pp. D32–D68.
4. A. Carvalho Multibody Dynamics Modelling and Analysis of the Human Hand *MASc Thesis* (University of Victoria, cap. 4, 2007), pp. 43–55.
5. B. Mirtich Impulse-Based Dynamic Simulation of Rigid Body Systems *Doctoral Thesis* (University of California at Berkeley, cap. 5, 1996) pp. 132–147.
6. Y. Wang On Impact Dynamics of Robotic Operations *Technical Report (CMU-RI-TR-86-14)* (Carnegie-Mellon University, 1986).
7. T. Liu and Y. Wang, "Computation of Multi-Rigid-Body Contact Dynamics," *Proceedings of the 2004 IEEE International Conference on Robotics and Automation* (New Orleans—, 2004), pp. 3220–3225.
8. Y. F. Zheng and H. Hemani, "Mathematical modeling of a robot collision with its environment", *IEEE Trans. Syst. Man Cybern.***14**(3) (1984).
9. A. Tornambé, "Global regulation of planar robot arm striking a surface," *IEEE Trans. Autom. Control* **41**(10), 1517–1521 (1996).
10. R. W. Cottle, J. S. Pang and R. E. Stone, *The Linear Complementarity Problem* (Academic Press, 1992).
11. M. Anitescu, S. K. Arason, V. I. Arnold and I. U. Bronshtein, "Formulating Dynamic Multi-Body Contact Problems with Friction as Solvable Linear Complementary Problems," *Reports on computational Mathematics, no. 93/1996* (Department of Mathematics, University of Iowa, USA, 1996).
12. D. Baraff, "Fast contact force computation for non-penetrating rigid-bodies," *Algorithmica* **10**, 292–352 (1994).
13. R. Featherstone, *Robot Dynamics Algorithms* (Kluwer Academic Publishers, Boston, MA, 1984).
14. S. McMillan, D. E. Orin and R. B. McGhee, "Efficient dynamic simulation of an underwater vehicle with a robotic manipulator," *IEEE Trans. Syst. Man Cybern.* **25**(3), 1194–1206 (1995).
15. R. Featherstone, "A divide-and-conquer articulated-body algorithm for parallel O(log(n)) calculation of rigid-body dynamics. Part 1: Basic algorithm," *Int. J. Robot. Res.* **18**(9), 867–875 (1999).
16. R. Featherstone, "A divide-and-conquer articulated-body algorithm for parallel O(log(n)) calculation of rigid-body dynamics. Part 2: Trees, loops and accuracy," *Int. J. Robot. Res.* **18**(9), 876–892 (1999).
17. K. S. Anderson and J. H. Critchley, "Improved 'Order-N' performance algorithm for the simulation of constrained multi-rigid-body dynamic systems," *Multibody Syst. Dyn.* **9**, 185–212 (2003).
18. K. Yamane and Y. Nakamura, "Parallel O(log N) algorithm for dynamic simulation of humanoid robots," *Proceedings of the HUMANOIDS'06 2006 IEEE-RAS International Conference on Humanoid Robots* (2006), pp. 554–559.
19. K. S. Anderson and S. Duan, "Highly paralelizable low order algorithm for the dynamics of complex multi-rigid-body systems," *AIAA J. Guid. Control Dyn.* **23**(2), 355–364 (2000).

https://doi.org/10.1017/S0263574710000524 Published online by Cambridge University Press